

**FABRICATION OF BISMUTH FERRITE/POLY(O-
PHENYLENEDIAMINE) BASED
CARBOXYMETHYL CELLULOSE HYDROGEL
AND ITS PHOTOCATALYTIC PERFORMANCE
TOWARDS METHYL ORANGE UNDER
DIRECT SUNLIGHT**

NOR ATILIA ATHIRA BINTI ZAAHARI

UNIVERSITI SAINS MALAYSIA

2022

**FABRICATION OF BISMUTH FERRITE/POLY(O-
PHENYLENEDIAMINE) BASED
CARBOXYMETHYL CELLULOSE HYDROGEL
AND ITS PHOTOCATALYTIC PERFORMANCE
TOWARDS METHYL ORANGE UNDER
DIRECT SUNLIGHT**

by

NOR ATILIA ATHIRA BINTI ZAAHARI

**Thesis submitted in fulfilment of the requirements
for the degree of
Master of Science**

October 2022

ACKNOWLEDGEMENT

In the name of Allah, Most Precious, Most Merciful. First of all, I praise Allah for making this journey possible.

I would like to express my gratitude to my research supervisor, Associate Professor Ts. Dr. Noor Haida Mohd Kaus for her invaluable advices, guidance and her enormous patience throughout the development of the research. Without her help, supportive motivation and suggestions, this journey will become harder. Thanks for providing lots of opportunity for me to attend conferences and colloquiums. These have definitely widened my perspective about scientific research and have been some of the greatest moment in my life.

I also want to express my deepest gratitude to my parents, Zaahari Bin Yaacub and Haniazah A' Esah Binti Muhd Isa for their endless support, physically, mentally and emotionally. Special thanks to my friends, Nur Anis Syazmin and Ahmad Fadhil for the unforgettable memories throughout the year. Real friendship does not expire. Hopefully, our friendship will last forever. Not forgetting my beloved husband, Ahmad Nazri Aziz, thank you for always being there for me.

I would also like to thank Universiti Sains Malaysia for providing me the Research University Grant (RUI) 1001/PKIMIA/8011069 that funds my master study.

Last but not least, I would like to thank School of Chemical Sciences for providing enough laboratory facilities for us to carry out my research project so that I could finish the project on time.

Nor Atilia Athira Zaahari

October 2022

TABLE OF CONTENTS

ACKNOWLEDGEMENT	ii
TABLE OF CONTENTS	iii
LIST OF TABLES	vii
LIST OF FIGURES	viii
LIST OF ABBREVIATIONS	xi
LIST OF APPENDICES	xiii
ABSTRAK	xiv
ABSTRACT	xv
CHAPTER 1 INTRODUCTION	1
1.1 Research Background.....	1
1.2 Problem Statement	4
1.3 Objectives of Study	4
1.4 Scope of Research	4
1.5 Significant of Study	5
1.6 Thesis Outline	5
CHAPTER 2 LITERATURE REVIEW	6
2.1 Type of Dyes	6
2.1.1 Anionic Dye	7
2.1.2 Methyl Orange	7
2.2 Technology of Dye Removal	8
2.3 Photocatalytic Degradation	9
2.3.1 Advance Oxidation Process	9
2.3.2 Photocatalytic Degradation of Dye	9

2.4	Photocatalyst	10
2.4.1	Bismuth Ferrite (BFO)	11
2.4.2	Synthesis Method of BFO	11
2.4.3	Application of BFO as Photocatalyst	12
2.4.4	Mechanism of Photocatalytic Degradation	13
2.4.5	Kinetic of The Photocatalyst	14
2.5	Conducting Polymer	16
2.5.1	Poly-o-phenylenediamine (PoPD) as Composite Material	17
2.6	Modification of Catalyst	18
2.6.1	Carboxymethyl Cellulose (CMC) as Support Material	19
CHAPTER 3 METHODOLOGY		21
3.1	Experimental Flowchart	21
3.2	Chemicals and Reagents	22
3.3	Preparation of CMC/BFO/PoPD Hydrogel Film	23
3.3.1	Synthesis of BFO Catalyst by Biotemplating Method	23
3.3.2	Synthesis of BFO/PoPD Composite by Oxidative Polymerization .	23
3.3.3	Optimization of BFO/PoPD Composite	24
3.3.4	Preparation of CMC Hydrogel Film	24
3.3.5	Impregnation of BFO/PoPD on CMC Hydrogel Film	25
3.4	Characterization of Materials	25
3.4.1	X-Ray Diffraction	25
3.4.2	X-ray photoelectron spectroscopy	26
3.4.3	Scanning Electron Microscopy with Energy Dispersive X-Ray	26
3.4.4	High Resolution Transmission Electron Microscopy (HRTEM)	27
3.4.5	Thermogravimetric Analysis	27

3.4.6	Attenuated total reflectance - Fourier Transform Infrared Spectroscopy	28
3.4.7	UV–Vis Diffuse Reflectance Spectroscopy	28
3.4.8	Determination of pH Point of Zero Charge	29
3.4.9	Material Surface Area and Porosity	29
3.5	Removal of Methyl Orange.....	30
3.5.1	Absorption Test.....	30
3.5.2	Influence Parameter of Photocatalytic Degradation	30
3.5.3	Kinetic Study.....	32
3.5.4	Reusability of CMC/BFO/PoPD Composite Film	32
CHAPTER 4 RESULTS AND DISCUSSION		34
4.1	Preparation of CMC/BFO/PoPD Hydrogel Film	34
4.1.1	Optimization of CMC Hydrogel Film.....	35
4.2	Characterization of Materials	38
4.2.1	X-Ray Diffraction	38
4.2.2	X-ray Photoelectron Spectroscopy.....	41
4.2.3	Scanning Electron Microscopy with Energy Dispersive X-Ray.....	43
4.2.4	High Resolution Transmission Electron Microscopy (HRTEM)	45
4.2.5	Thermogravimetric Analysis.....	46
4.2.6	Fourier Transform Infrared Spectroscopy.....	50
4.2.7	Diffuse Reflectance Spectroscopy	53
4.2.8	Material Surface Area and Porosity	55
4.3	Removal of Methyl Orange.....	59
4.3.1	Adsorption study	59
4.3.2	Optimization of BFO/PoPD Composite.....	60
4.3.3	Influence Parameter of Photocatalytic Degradation	64

4.4	Kinetic Study.....	71
4.5	Reusability of CMC/BFO/PoPD Composite Film.....	72
4.6	Post Treatment Analysis	74
4.7	Proposed Removal Mechanism.....	75
CHAPTER 5 CONCLUSION		77
REFERENCES.....		79
APPENDICES		

LIST OF TABLES

	Page
Table 2.1 List of Photocatalyst.....	10
Table 4.1 Summary of FTIR absorption bands	52
Table 4.2 BET surface area of BFO and BFO/PoPD.....	58

LIST OF FIGURES

		Page
Figure 2.1	Molecular structure of MO.....	8
Figure 2.2	Mechanism of photocatalyst	14
Figure 2.3	Mechanism of Crosslinked CMC.....	20
Figure 3.1	Experimental Flowchart	22
Figure 4.1	Schematic reaction of oPD to PoPD	35
Figure 4.2	Image of (a) BFO/PoPD, (b) CMC film and (c) CBP hydrogel film.....	35
Figure 4.3	Gel fraction of CMC by varying 4 parameters; (a) ratio of CMC: citric acid, (b) drying temperature, (c) curing time and (d) curing temperature.....	38
Figure 4.4	XRD pattern of (a) PoPD, (b) BFO, (c) BFO/PoPD and (d) CBP film	40
Figure 4.5	X-ray photoelectron spectra of (a) Bi 4f, (b) Fe 2p, (c) O 1s, (d) C 1s, and (e) N 1s peaks in CBP composite photocatalyst.....	42
Figure 4.6	SEM Image of (a) BFO, (b) PoPD, (c) BFO/PoPD, and (d) BSE image of CBP	44
Figure 4.7	Image of (a-g) EDX mapping of CBP film and (h) EDX of composition CBP	45
Figure 4.8	HRTEM images of (a-b) CBP hydrogel film, (c) lattice fringes, and (d) selected-area electron diffraction pattern of the CBP hydrogel film	46
Figure 4.9	Thermogram of BFO with DTG curve	47
Figure 4.10	Thermogram of BFO/PoPD with DTG curve	48

Figure 4.11	Thermogram of CMC with DTG curve	49
Figure 4.12	Thermogram of CBP film with DTG curve	50
Figure 4.13	FTIR spectra of (a) PoPD, (b) BFO, (c) BFO/PoPD and (d) CMC and CBP hydrogel film	53
Figure 4.14	Band gap energy of (a) BFO, (b) BFO/PoPD and (c) CBP hydrogel film	55
Figure 4.15	Linear sorption isotherm of (a) BFO, (b) BFO/PoPD and (c) CBP hydrogel film.....	57
Figure 4.16	Removal efficiency of dye using BFO, BFO/PoPD, CMC, CBP in the absence of light	59
Figure 4.17	Removal efficiency of MO with different ratio of BFO to oPD, $[MO]_0$ = 10 ppm, 0.01 g catalyst loading on CMC film.....	61
Figure 4.18	Removal efficiency of MO with different concentration of HCl during polymerization of oPD, $[MO]_0$ = 10 ppm, 0.01 g catalyst loading on CMC film	62
Figure 4.19	Removal efficiency of MO with different ratio of APS to oPD, $[MO]_0$ = 10 ppm, 0.01 g catalyst loading on CMC film.....	64
Figure 4.20	Removal efficiency of MO with different amount of catalyst loading on CMC vs irradiation time, $[MO]_0$ = 10 ppm.....	66
Figure 4.21	Removal Efficiency of MO with different initial concentration vs irradiation time using 0.01 g of BFO/PoPD on CMC hydrogel film.....	68
Figure 4.22	Plot of pH_{PZC} of CBP film composite after 24 hours.	69
Figure 4.23	Removal of MO dye within 140 min (50 mL, $[MO]_0$ = 10 ppm using 0.01 g of BFO/PoPD on CMC film.....	71

Figure 4.24	Removal efficiency of MO for five cycle, 0.01 g catalyst loading, [MO] ₀ = 10 ppm, unadjusted pH.....	73
Figure 4.25	The condition of the CBP hydrogel film after 5 th cycle of reusability	74
Figure 4.26	(a) FTIR spectra and (b) XRD patterns of CBP hydrogel film before and after the removal of MO (0.01 g of catalyst loading, 10 ppm of [MO], unadjusted pH solution)	74
Figure 4.27	Proposed removal mechanism of MO.....	76

LIST OF ABBREVIATIONS

AOP	Advance Oxidation Processes
APS	Ammonium Persulphate
BE	Binding Energy
BET	Brunauer, Emmett and Teller
BFO/BiFeO ₃	Bismuth Ferrite
BSEI	Backscattered electron image
CA	Citric Acid
CB	Conduction Band
CMC	Carboxymethyl Cellulose
CBP	CMC/BFO/PoPD hydrogel film
CR	Congo Red
CV	Crystal Violet
DRS	Diffuse Reflectance Spectroscopy
DTG	Differential Thermogram
FACs	Fly-ash Cenospheres
FTIR	Fourier Transform Infrared Spectroscopy
HOMO	Highest Occupied Molecular Orbital
HRTEM	High Resolution Transmission Electron Microscopy
ICPs	Intrinsically conducting polymer
IUPAC	International Union of Pure and Applied Chemistry
L-H	Langmuir-Hinshelwood
LNR	Linear Natural Rubber
LUMO	Lowest Unoccupied Molecular Orbital
MB	Methylene Blue
MO	Methyl Orange
oPD	o-phenylenediamine
PA	Polyacetylene
PAN NFs	Polyacrylonitrile Nanofibres
PANI	Polyaniline
PANI/SnS	Polyaniline-modified 3D-spongy SnS
PEDOT	Poly(3,4-ethylenedioxythiophene)

pH _{PZC}	pH of Point of Zero Charge
PoPD	Poly-o-phenylenediamine
PPy	Polypyrrole
PTh	Polythiophene
RhB	Rhodamine B
S _{BET}	BET Surface Area
SEM-EDX	Scanning Electron Microscopy- Energy Dispersive X-Ray
SEI	Secondary electron image
TGA	Thermogravimetric Analysis
UV-VIS	Ultraviolet-Visible Spectroscopy
VB	Valence Band
XPS	X-Ray Photoelectron Spectroscopy
XRD	X-Ray Diffraction

LIST OF APPENDICES

- APPENDIX A BET SURFACE AREA OF (A) BFO AND (B) BFO/POPD
- APPENDIX B LINEAR FIT OF FIRST ORDER REACTION OF MO
REMOVAL USING CBP HYDROGEL FILM
- APPENDIX C CALIBRATION CURVE OF METHYL ORANGE (pH
UNADJUSTED)

**PEMFABRIKAN BISMUT FERIT/POLI(O-FENILINADIAMINA)
BERASASKAN HIDROGEL KARBOSIMETIL SELULOSA DAN PRESTASI
FOTOPEMANGKINNYA TERHADAP METIL JINGGA DI BAWAH
CAHAYA MATAHARI LANGSUNG**

ABSTRAK

Filem hidrogel CMC/BFO/PoPD (CBP) telah berjaya disediakan dengan mengisi tepu BFO/PoPD yang telah dioptimumkan ke dalam hidrogel karbosimetil selulosa (CMC) menggunakan keadaan nisbah molar BFO:oPD 1:0.4 di dalam 0.1 M HCl dan nisbah molar antara ammonium persulfat (APS) kepada oPD iaitu 1.5:1 untuk menyingkirkan pewarna metil jingga (MO) di bawah cahaya matahari langsung. Sampel CBP telah dicirikan oleh pembelauan sinar-X (XRD), spektroskopi fotoelektron sinar-X (XPS), pengimbasan elektron mikroskopi dengan tenaga serakan sinar-X (SEM-EDX), mikroskop elektron penghantaran resolusi tinggi (HRTEM), analisis gravimetri terma (TGA), spektroskopi pantulan keseluruhan dikecilkan-fourier transformasi inframerah (ATR-FTIR), spektroskopi pantulan baur UV-sinar nampak (DRS) dan analisis penjerapan N₂. Analisis XRD, gambar SEM dan HRTEM menunjukkan rangkuman BFO/PoPD di dalam medium CMC. Luang jalur bagi filem hidrogel CBP telah dikira menggunakan persamaan Kubelka Munk dengan nilai 2.09 eV. 93% MO telah terdegradasi setelah 140 minit tindak balas dengan pemuatan BFO/PoPD sebanyak 0.01 g di dalam komposit CBP. Disebabkan penyingkiran MO didominasi oleh proses fotodegradasi, proses penyingkiran itu mengikuti model kinetik Langmuir-Hinshelwood. CBP dapat menyingkirkan MO melebihi 70% selepas kitaran kedua dan kekal lebih 50% selepas kitaran ke-5 tanpa memerlukan proses pemisahan rawatan-lepas. Oleh itu, ia lebih bagus bagi aplikasi perindustrian.

**FABRICATION OF BISMUTH FERRITE/POLY(O-PHENYLENEDIAMINE)
BASED CARBOXYMETHYL CELLULOSE HYDROGEL AND ITS
PHOTOCATALYTIC PERFORMANCE TOWARDS METHYL ORANGE
UNDER DIRECT SUNLIGHT**

ABSTRACT

CMC/BFO/PoPD (CBP) hydrogel film is successfully prepared by impregnating of the optimized BFO/PoPD into carboxymethyl cellulose (CMC) hydrogel with condition of molar ratio of BFO:oPD was 1:0.4 in 0.1 M HCl and the molar ratio of ammonium persulphate (APS) to oPD was 1.5:1 for degradation of methyl orange (MO) under direct sunlight. The CBP sample was characterized by X-ray diffraction (XRD), X-ray photoelectron spectroscopy (XPS), scanning electron microscope with energy dispersive X-ray (SEM-EDX), high resolution transmission electron microscopy (HRTEM), thermogravimetric analysis (TGA), attenuated total reflectance-fourier transform infrared (ATR-FTIR) spectroscopy, UV-Vis Diffuse Reflectance Spectroscopy (DRS) and N₂ adsorption analysis. The XRD pattern, SEM image and HRTEM image revealed the inclusion of BFO/PoPD within CMC medium. The band gap of the CBP hydrogel film was calculated utilising Kubelka Munk equation with value of 2.09 eV. 93% of MO was degraded within 140 min reaction with BFO/PoPD loading of 0.01 g in CBP composite As MO removal is selectively governed by photodegradation, the removal process follows Langmuir-Hinshelwood kinetic model. CBP was able to degrade MO above 70% after second cycle and maintained above 50% after 5th cycle with unnecessary of post treatment separation step. Therefore, it is advantageous for industrial application.

CHAPTER 1

INTRODUCTION

1.1 Research Background

One of the greatest environmental challenges in the world today is water pollution caused by the discharge of coloured effluents mainly from textile dyeing industries which released around 8–20% of unutilized dyes and auxiliary chemicals into the wastewater stream [1]. The discharge of these dyes into effluents has an impact on people who use these effluents for daily activities such as washing, bathing, and drinking. As a result, it is critical to check the water quality, especially since even 1.0 mg/L of dye concentration in drinking water can impart a substantial colour, rendering it unsafe for human consumption. Methyl orange (MO) is an organic dye that has been used in the textile industry and can be found in wastewater. Due to its chemical structure, MO is resistant to fading on exposure to light, water and chemical, therefore, difficult to decolourised [2,3]. This anionic dye is highly toxic which is harmful to environment and human health causing various disease and disorder [4,5]. Hence, its removal from aquatic wastewater is a crucial step. Various traditional physical techniques have been employed to treat the wastewater such as reverse osmosis, coagulation, precipitation, adsorption on activated carbon and membrane filtration [6–8]. However, these methods have creating secondary pollution because the pollutants are just transferred to another phase; thus, further treatment of solid waste is needed [9,10].

Advanced oxidation processes (AOPs), which can be utilised to turn harmful and resistant compounds into ecologically benign minerals, is one of the latest alternative technologies for wastewater treatment. One of the most efficient AOPs is catalytic oxidation, which is based on the active radicals generated during a reaction

in the presence of a catalyst under very mild reaction conditions. The efficiency of photocatalysts in treating wastewater, discovered by Fujishima and Honda in 1972, has piqued the interest of researchers due to their low cost and reusability. Up to the present, numerous studies have been done on titanium dioxide (TiO_2) [11,12], zinc oxide (ZnO) [13] and cerium (IV) oxide (CeO_2) [14] owing to their semiconductor properties. However, due to the large band gap, these photocatalysts are located in the UV-light region of the solar spectrum. Bismuth ferrite, BiFeO_3 (abbreviated as BFO), on the other hand, has long been used in magnetism, spintronics, and photovoltaics due to its magnificent multiferroic and ferroelectric characteristics at ambient temperature. Owing to its narrow band gap of ~ 2.2 eV, BFO has recently emerged as a potential visible-light driven photocatalyst [15]. Furthermore, it has high chemical stability, recyclable, and is created from renewable resources. Nevertheless, the reported photocatalytic activity of BFO is still low because of the rapid recombination of photogenerated electron-hole pairs in BFO. The efficiency of pristine BFO were observed to be too low towards the degradation of anionic dyes such as MO even under dark or direct sunlight [16]. Therefore, strategies are needed for improvement of the photocatalytic activity of BFO.

Typically conducting polymer has attracted considerable attention since its discovery. The properties of conducting polymer in electron transfer processes have been extensively studied to demonstrate efficient arouse a rapid photo-induced charge separation and a relatively slow charge recombination [17]. Polyaniline (PANI), polypyrrole (PPy), polythiophene (PTh), and polyfuran are examples of intrinsically conducting polymers (ICPs) that conduct electricity due to the presence of delocalized π -electrons [18–21]. These ICPs are being studied for usage as alternatives for inorganic electronic, opto-electronic, and semiconducting materials due to their

processability, adjustability, and environmental stability [22,23]. Among them, aromatic diamine polymer like poly(o-phenylenediamine) (PoPD) has attracted more researchers' interest because it has high synthesizability, better doping ability, high thermal stability and strong electro-activity due to the presence of a large number of free amino groups. Therefore, they can be easily bonded with inorganic nanoparticles [24,25].

Furthermore, as the semiconductors have small particle sizes, the separation may be time consuming and lead to catalyst loss. Low catalyst recovery and reusability will result from the latter drawback. Therefore, continuous efforts have been made to support catalyst on various substrates namely glass mats, fabrics, and polymers. Cellulose is one the natural polymers which is renewable, allowing for the development of environmentally beneficial and cost-effective solutions through the functionalization of these polymers. In this sense, cellulose-rich biomass is extremely important as a chemical feedstock since it contains cellulose, hemicelluloses, and lignin, all of which contain functional groups appropriate for functionalization [26,27]. Solid waste of oil palm empty fruit bunch, water hyacinth, annual plants like *M. sinensis*, *E. crassipes* and *C. papyrus* are the examples of biomass resources of cellulose. Carboxymethyl cellulose (CMC) is a derivative of cellulosic compound which soluble in water at room temperature [28]. This natural polymer has been chosen as an immobilizer or support material for BFO/PoPD photocatalyst prior to great mechanical properties, high adsorption capacity and good compatibility within the system. According to prior research, the application of PoPD as a composite for BFO for dye photodegradation under solar light irradiation has not been extensively studied.

1.2 Problem Statement

BFO is discovered as visible-light responsive photocatalyst due to its narrow band gap. However, to date, not so much studies of photocatalytic activity of BFO have been reported due to rapid recombination of photo-generated electron-hole pairs in BFO. The recombination of photo-generated electron-hole pairs might be decreased by forming electron- or hole-trapping centres within the photocatalyst lattice. In this study, PoPD, which has been studied for its efficient rapid photo-induced charges separation and relatively slow charge recombination, has been chosen to be as support catalyst. However, there is a high chance to lost photocatalyst after the water treatment due to the powder form of photocatalyst. Therefore, the photocatalyst needs to be immobilized to avoid losing to the water without jeopardising its photocatalytic activity. To cope with this issue, CMC has been chosen to be an immobilizer for BFO/PoPD photocatalyst in the thin film form, as it has high adsorption capacity as well as good mechanical properties. Therefore, owing to the properties of the chosen material, the fabrication of CBP hydrogel film will shows an excellent photocatalytic degradation of MO as the pollutant model in this study.

1.3 Objectives of Study

1. To synthesize and optimized BFO/PoPD composite and CBP hydrogel film
2. To characterize BFO/PoPD and CBP hydrogel film
3. To investigate photocatalytic activity, kinetic and stability of CBP hydrogel film of MO under direct sunlight.

1.4 Scope of Research

The goal of this study is to effectively treat water pollution using an anionic dye as the pollutant model. The treatment of dye effluents is proposed to be done via photocatalysis using CBP hydrogel film. BFO will be synthesized via biotemplated

method and BFO/PoPD will be synthesized and optimized by oxidative polymerization. This composite will be impregnated on CMC membrane as support material. To comprehend the characteristic and development of the material, many characterisation procedures are performed.

1.5 Significant of Study

The fabrication of CBP composite as photocatalyst was proposed for efficient photocatalytic degradation of MO under direct sunlight. Very few studies on the BFO were reported and the process of CBP composite for photocatalytic degradation of anionic dye under visible light has not been explained elsewhere. The idea of this research work indicated composite photocatalyst with excellent photocatalytic performance owing to the sensitizing effect of PoPD as conducting polymer, and the synergetic effect between conducting polymer and BFO. In order to improve the recovery and reusability of the catalyst, CMC was used as a catalytic support or immobiliser.

1.6 Thesis Outline

This study consists of five chapters, which present the research in sequential order. Chapter 1 introduces the research background, problems statement, objectives, scopes, and significant of this research. In Chapter 2, the literatures on dyes and recent issues about the photocatalyst are reviewed. Chapter 3 outlines the experimental methodology and characterization of the photocatalyst whereas Chapter 4 analyzes and discusses the characterization and experimental data. Finally, the conclusion and recommendation for future were presented in Chapter 5.

CHAPTER 2

LITERATURE REVIEW

2.1 Type of Dyes

Dyes usually have many structural varieties and their complete classification with respect to one parameter is very difficult and of no use from practical understanding point of view. However, dyes are generally divided into different groups and classes depending on their source, general dye structure and the fiber type with which they are most compatible. Among major dye categories, azo dyes are the largest group of colourants and over 50% of all the dyes used in industries are azoic dyes. Moreover, they have amphoteric properties due to the presence of additional carboxyl, hydroxyl, amino or sulfoxyl functional groups. Azo dyes can behave anionic (deprotonation at the acidic group), cationic (protonated at the amino group) or non-ionic depending upon the pH of the medium [29].

Generally, dye molecules consist of two main components; chromophores and auxochromes. Chromophores are responsible in providing colour while auxochromes increase the dye's affinity for fibres. Dyes based on general structure can be classified as: cationic, anionic, and non-ionic. Cationic dyes are basic dyes like methylene blue (MB) and crystal violet (CV), whereas anionic dyes are direct, acidic, and reactive dyes like methyl orange (MO) and congo red (CR). Unlike anionic dye, which is extremely stable in water, cationic dyes are able to degrade itself and this phenomenon known as photolysis. Major nonionic dyes include; disperse dyes which does not ionizes in the aqueous environment and the major cationic dyes include basic and disperse dyes [29–32].

2.1.1 Anionic Dye

Anionic dyes depend on a negative ion that includes many compounds from the most varied classes of dyes, which have specific structural distinctions (e.g., azoic, anthraquinone, triphenylmethane and nitro dyes). However, all anionic dyes contain anionic functional groups, for instance, sulfonic or carboxylic acid groups. These functional groups are water-soluble and can effectively interact with photocatalysts with hydrophilic surfaces [33]. Around half of all known dyes are anionic azo dyes, making them the most abundant group of synthetic dyes and the most often emitted into the environment [30,34].

2.1.2 Methyl Orange

MO is an example of azo dyes containing chromophore ($-N=N-$) in its molecular structures as in Figure 2.1, MO changes color from red to orange-yellow at pH values between 3.1 and 4.4. Currently, more than half of the dyes and inks are azo in nature which has been used widely for textile, dyeing and paper painting due to their colour versatility and low cost [35,36]. Textile industries, for instance, use 30% of dyes and 17-20% of them were discharged into lakes, rivers, or ground waters during the dyeing process and became water pollution [2,5,12]. The chemical bonding of this dye cannot be easily break and tend to form toxic and carcinogenic compounds over time. However, these compounds are also commonly used as indicators or for histological staining. MO is considered an allergenic material, in contact with the skin. If ingested, it can cause rashes or even intoxication [36].

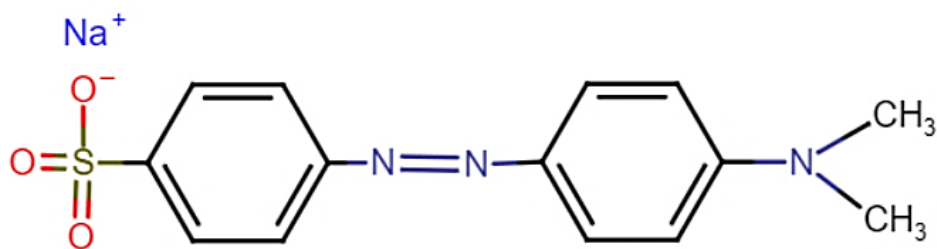


Figure 2.1 Molecular structure of MO

2.2 Technology of Dye Removal

Currently, the disposal of waste generated by various human activities is a major issue for society. During the last decades, it has been clear that residues from domestic, agricultural, and industrial activities must be removed before they become environmental pollutants. Water pollution, in particular, can cause serious epidemiological problems in receiving bodies such as rivers, lakes, underground currents, and the sea, as well as in the field of environmental and human health. This global issue has necessitated the search for alternative wastewater treatment technologies based on chemical, biological, or physical methods.

Chemical methods such as ozonation [37], oxidation [38], electrolysis [39] and physical method like adsorption [40], coagulation-flocculation [41], and membrane technologies [42] have been employed to remove colours from textile effluents. oxidise or decrease organic and inorganic chemicals by utilising the metabolic activities of bacteria, archaea, fungi, algae, or plants [10]. However, these treatment methods for the removal of dyes from the waste water suffer from some drawback which only transfers the dyes from one stage to another, hence generating secondary pollution [32].

2.3 Photocatalytic Degradation

2.3.1 Advance Oxidation Process

Many studies have been conducted in order to develop a better treatment process as conventional physical and biological processes are time consuming, require large space, pH sensitive and inefficient against non-biodegradable harmful pollutants. It is also incapable of treating wastewater with high concentrations of contaminants [43,44]. Thus, the advanced oxidation process (AOP) offers an alternate way to assist remove these contaminants in the wastewater treatment system because it can mineralize pollutants through redox reactions into safer molecules.

AOP is a method that uses oxidizing agents such as hydroxyl radical (OH^{\bullet}), superoxide radical ($\text{O}_2^{\bullet-}$), and sulphate radical ($\text{SO}_4^{\bullet-}$) to degrade refractory pollutants in wastewater treatment plants [45]. The processes are mainly based on non-selective character of reaction of hydroxyl radicals (HO^{\bullet}) having high oxidation potential with organic pollutants at high reaction rates (generally between 10^8 – $10^{11} \text{ M}^{-1}\text{s}^{-1}$). These processes are therefore capable for the oxidation of many pollutants [43].

2.3.2 Photocatalytic Degradation of Dye

Photocatalysis has received substantial attention as one of the most promising environmental clean-up technologies among numerous AOPs; yet, its cost competitiveness remains lower than conventional treatment techniques. Many researchers have attempted to degrade the dye via photocatalysis. Bhatti et. al. successfully degraded 88% of 16.4 ppm MO by using silver doped ZnO nanorods within 120 min under UV light [2]. Meanwhile, by using 0.05 g of Ag/TiO₂, Zheng and co-workers degraded 65.4% of 7.5 ppm MO within 120 min under solar simulation. Similarly, Chen and colleagues had done a flourishing work by degrading 99.7% of 30 ppm MO within 30 min using 0.01 g of ZnO under UV light [46].

2.4 Photocatalyst

Photocatalyst is a catalyst that converts photons (light) into chemical energy to initiate a catalytic process. The catalytic process is governed by several critical properties such as the band gap (semiconductor), surface area, shape, reusability, and stability, all of which contribute to the achievement of the necessary photocatalytic activity. In addition, there are other properties such as light absorption, biocompatibility, and the ability to generate charge carriers when stimulated with the required amount of light energy all play a role in selecting an appropriate catalyst. Numerous semiconductors have been extensively investigated for their photocatalytic properties, including titanium [11,47], vanadium [48], tin [34], and zinc [46] which are abundant in nature. As time goes on, researchers are becoming more interested in photocatalysts with narrow band gaps that may use direct sunshine instead of UV radiation to lower the cost of photocatalytic reaction. Table 2.1 shows some examples of catalyst which have been used to degrade the dye as the pollutant model.

Table 2.1 List of Photocatalyst

Catalyst	Pollutant	[Pollutant] (ppm)	Dosage (g/L)	Time (min)	Source of light	% Removal	Ref.
PoPD/ TiO ₂	MB	10	0.01	180	Visible light	85.9	[49]
ZnO/Ag	MO	16	1	250	Visible light	95.2	[50]
PANI/ SnS	MO	15	0.03	120	Visible light	81.4	[34]
La ₂ NiO ₃ / ZnO	MO	10	0.05	60	Visible light	90	[51]
Ag/AgCl -CMC	RhB	10	4	60	Visible light	60	[52]
Ag/ TiO ₂	MO	7.5	0.05	120	Visible light	65.4	[53]
ZnO	MO	30	0.01	30	UV light	99.7	[46]
CBP	MO	10	0.01	140	Visible light	93	This work

2.4.1 Bismuth Ferrite (BFO)

Bismuth ferrite, BFO, is a perovskite oxide, act as a promising visible light photocatalyst which attracted most researchers' interest. It is a one-of-a-kind multiferroic semiconductor having both ferroelectric and ferromagnetic characteristics, resulting in bulk photovoltaic effect, in which photocurrent can flow uniformly throughout the material without forming an interface. The ferroelectricity is caused by the stereochemistry of the lone pair from bismuth atoms [54–56]. These qualities are characterized by the presence of an electric polarization, magnetization, or elastic deformation, which may be switched abruptly by the action of an electric field, a magnetic field, or straining, respectively [57]. Taking advantages of its high phase transition temperatures ($T_{\text{Néel}} = 370 \text{ }^\circ\text{C}$; $T_{\text{Curie}} = 873 \text{ }^\circ\text{C}$), BFO is one of the few known materials that can be utilised as a multiferroic at ambient temperature and shows a rhombohedrically distorted perovskite structure belonging to the special group R3c (α -BiFeO₃ phase).

2.4.2 Synthesis Method of BFO

The method for synthesizing pure BFO is still discussed in literature such as hydrothermal [58], sol gel [59,60], microwave [61], ultrasonic [62] and biotemplate method [54,55,63]. However, the different method used to synthesize BFO had produced different morphology and size as well as the presence of impurities and synthesis method used is depending on the application of BFO. Recently, the biotemplate technique has piqued the interest of researchers seeking to synthesize nanomaterials due to its ability to create highly organised morphology and topology of nanomaterials. A biotemplate is a pattern or mould obtained from biological resources that contain preferred chelation sites from polysaccharide functional groups (amine, carboxylate, hydroxyl, or amide groups) within molecular structures [56,64].

Yan et. al., had successfully prepared a mesoporous TiO₂/SiO₂ composite by utilizing biotemplate from aquatic plant for the degradation of gentian violet. Their prepared biotemplate TiO₂/SiO₂ has a higher specific surface area than Degussa P25, thus, better photocatalytic activity [65]. On the other hand, Satar et. al. victoriously synthesized a rhombohedral distorted structure phase BFO by employing κ-carrageenan as biotemplate. As a result, they found that BFO nanoparticles were more uniform, dense and homogeneous in shape [56].

2.4.3 Application of BFO as Photocatalyst

Along with their unique characteristics, BFO materials have enormous promise for creating and developing a wide range of devices with novel functions in the field of electronics, spintronics, and photonics devices. In addition to its wide applications, BFO is also well-known in the photocatalysis area due to its narrow band gap which lying in the visible part of the solar spectrum and making BFO a viable photocatalyst harnessing solar energy for treating contaminated wastewater and/or split water for hydrogen production. Jiang et. al. investigated the photocatalytic activity of BFO by using 10 ppm of rhodamine B (RhB) under visible light from Xe lamp. 90.5% of RhB was successfully degraded after four hours in the presence of H₂O₂ [58]. Soltani et. al. also used RhB as their pollutant model to study the efficiency of BFO. They successfully degraded approximately 70% of the total organic carbon by utilizing 50 g/L of BFO within 35 min under sunlight irradiation [62].

Researchers are also actively trying to modified BFO with dopant due to its drawback; fast recombination rate. For instance, Malathi and colleagues proposed BFO incorporated bismuth oxyiodide via wet impregnation process to study the photocatalytic degradation of RhB dye under visible light of the tungsten halogen lamp. It was found that, the composite degraded remarkably ~100 % of RhB in 120

min, compared to 10% of pure BFO [66]. Meanwhile, Wang et. al. fabricated Zr-BFO photocatalyst and investigated its photocatalytic activity by employing 5 ppm MO as the pollutant candidate under visible light irradiation. The investigation had revealed, 87% of MO was successfully degraded after four hours reaction by using 0.2 g of composites compared to 40% degradation when using pristine BFO [67].

2.4.4 Mechanism of Photocatalytic Degradation

Ajmal et al. comprehensively studied the mechanism of semiconductor-supported photocatalyst. BFO is a photocatalyst that absorbs ultraviolet (UV) light from the sun. When irradiated by sunlight, the valence electron is activated and excited, forming the positive hole (h^+) in BFO's valence band (VB). In the VB, h^+ can produce hydroxyl radicals ($\bullet OH$) when it reacts with adsorbed H_2O molecules or an OH^- group. Meanwhile, the excited negative electron (e^-) is promoted to the lowest range of the BFO's unoccupied electronic band structure, called the conduction band (CB). Where there is dissolved oxygen, e^- can react with it to create superoxide radicals ($O_2\bullet$) and hydrogen peroxide (H_2O_2). This is known to as the photo-excitation state, and it is at this stage that the e^- and h^+ pairs are formed. This cycle is repeated in relation to the availability of photons (light) [29,68]. The mechanism of photocatalyst is illustrated as in Figure 2.2. The energy difference between the VB and the CB is known as the band gap energy of the photocatalyst which can be calculated by using Kubelka Munk equation as stated in Equation 2.1,

$$f(R) = \frac{(1-R)^2}{2R} = \frac{k}{s} \quad \text{Equation (2.1)}$$

Where R is the absolute reflectance of the sampled layer, k is the molar absorption coefficient and s is the scattering coefficient.

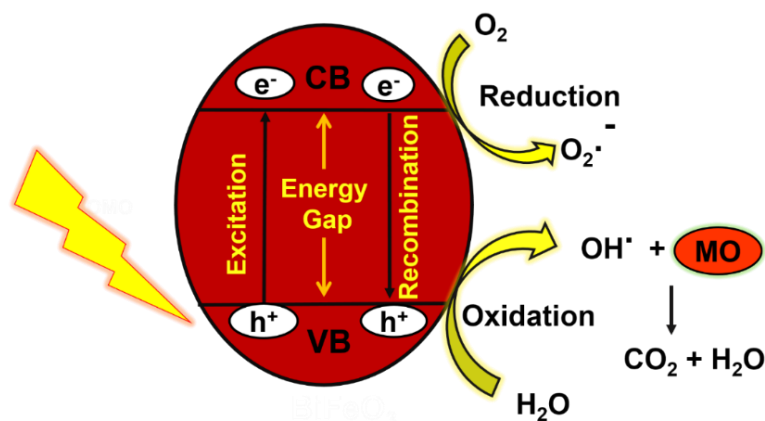


Figure 2.2 Mechanism of photocatalyst

2.4.5 Kinetic of The Photocatalyst

There is variety expression to study the kinetic of heterogeneous catalytic system including Langmuir-Hinshelwood (L-H), pseudo first-order and pseudo second order. The predicted photocatalytic degradation kinetics from L-H kinetic expression is compared with predicted kinetics from pseudo-first-order kinetic expression. In addition, the experimental kinetic data were also fitted to the second-order model and the best-fit kinetic model was selected based on the coefficient of determination, R^2 value. L-H kinetics have been reported for the heterogeneous catalytic degradation of several dye aqueous solutions using Equation 2.2.

$$r = -\frac{dC}{dt} = \frac{kKC}{1+KC} \quad \text{Equation (2.2)}$$

The pollutant concentration (mg/L) was indicated as C, where r represents the pollutant's photocatalytic degradation rate (mg/L min). The illumination duration, reaction rate constant (mg/L min), and pollutant adsorption coefficient (L/mg) are denoted by t, k, and K, respectively. Equation can be changed to the following equation if C was small,

$$r = -\frac{dC}{dt} = kC \quad \text{Equation (2.3)}$$

Where k (min^{-1}) represented the rate constant of reaction (first order). The rate constant, can be obtained through a linear fit from the plot of $\ln C_0/C$ versus irradiation time. If it set assumption $t = 0$, $C = C_0$, equation can be rewritten by the following equation:

$$\ln \frac{C}{C_0} = kt \quad \text{Equation (2.4)}$$

Where C_0 and C represented the pollutant concentration at time zero and t , respectively [69]. For instance, Lahmar et.al. study kinetic of the removal of MO by utilising ZnO supported lanthanum nickelate ($\text{La}_2\text{NiO}_4/\text{ZnO}$) under sunlight. They found that, the kinetics of degradation follows a first order reaction with an apparent constant of 0.022 min^{-1} [51]. Satar et. al. degraded MB by employing BFO and they found that the photocatalytic rate (k) was 0.0170 min^{-1} , which follow first order reaction [70].

Pseudo-first-order kinetics have also been widely reported by several researchers for heterogeneous catalytic dye degradation systems. The expression for pseudo first order is as in Equation 2.5,

$$q_t = q_e (1 - \exp^{-k_1 t}) \quad \text{Equation (2.5)}$$

For instance, the study of adsorption of MO by Mohammad et.al were well described by the pseudo-first order utilising chitosan-glyoxal/ TiO_2 nanocomposite with value 416.1 mg/g [4]. Meanwhile, Nagar et. al. employs silver nanoparticle (AgNPs) to degrade Mo in presence of peroxodisulphate and they found that, the reaction follows pseudo-first order kinetic with rate $15.9 \times 10^{-4} \text{ s}^{-1}$ [9].

In the other hand, Capanema and colleagues found that the adsorption kinetics of MB by CMC hydrogel was best described by the pseudo-second-order kinetics

model ($R^2 = 0.991$) which is expressed by Equation 2.6 and the integration of when $qt = 0$ at $t = 0$ leads to Equation 2.7. The rate constant calculate from Equation 2.7 was $0.0189 \text{ g.mg}^{-1}.\text{min}^{-1}$ [71].

$$\frac{dq(t)}{dt} = k(q_e - q(t))^2 \quad \text{Equation (2.6)}$$

$$\frac{t}{q(t)} = \frac{1}{kq_e^2} + \frac{t}{q_e} \quad \text{Equation (2.7)}$$

Where: k is the pseudo-second-order rate constant ($\text{g.mg}^{-1}.\text{min}^{-1}$) and q_e and $q(t)$ are the amounts of adsorbed dye (mg.g^{-1});

2.5 Conducting Polymer

Conducting polymers (CPs) are conjugated organic structures with alternating double and single bonds and delocalized π -electrons and this delocalization contribute to the generation of charge carriers like polarons, bipolarons, solitons, which are responsible for the insulator-metal transition. CPs have a wide range of applications due to their unique electrochemical and optical characteristics [72]. Polyaniline (PANI) [61,73], poly(3,4-ethylenedioxythiophene) (PEDOT) [74], polyacetylene (PA) [75], polypyrrole (PPy)[19], polyfuran (PF) [21], polythiophene (PTh) [20], and their derivatives are the common types of CPs.

PANI and its derivatives are the most promising support catalyst due to their high stability, processability, tuneable conductivity, increased doping ability, environmental stability, wide applicability, and optical properties. The PANI backbone consists of both quinoid and benzoid rings. Extensive efforts have been undertaken to enhance polyaniline processability by creating polyaniline derivatives with ortho- and meta-substituted groups, such as $-\text{OCH}_3$, $-\text{CH}_2\text{CH}_3$, $-\text{CH}_3$, $-\text{SO}_3\text{H}$, and so on. However, ortho-isomer is preferred over the meta-isomer for polymer synthesis since it exhibits a greater yield and conductivity than meta-isomer due to the repulsion

factor [22,24]. Recent research has focused on the synthesis of polyaniline derivatives with free active functional groups like $-NH_2$ and $-OH$ in the backbone chain, which can provide better solution processability, better doping by various dopants, and boosted performance in a wide range of applications. However, the presence of dopant has no effect on its chemical properties and does not result in the formation of a bond with the main chain; it exists in close proximity to the polymer chain [72].

2.5.1 Poly-o-phenylenediamine (PoPD) as Composite Material

Nowadays, many studies used polymers like PANI, PpPD, PoPD and etc. have been applied for modification of semiconductors. Taking advantages to its high conductivity, exceptional air stability, and unique physical and chemical characteristics when compared to other conducting polymers, PoPD is one of the most studied conducting polymers and has piqued the interest of many researchers working on a variety of practical applications. When combined with semiconductors, conductive polymers with extended π -conjugated electron structure could improve the photocatalytic activity in visible part of the spectrum [76].

Some researchers have been studied PoPD as support catalyst for photocatalyst. For example, Ye et. al. did flourish work when the band gap synthesized PoPD/ $ZnWO_4$ supported on the fly-ash cenospheres (FACs) reduced to 2.69 eV from 2.86 eV ($ZnWO_4$ /FACs) with enhanced photocatalytic performance under visible light. The investigation revealed that 76.7 % of tetracycline as pharmaceutical waste model was degraded under visible light. The results convince that PoPD plays an important role in the improvement of photocatalytic activity of $ZnWO_4$ [76]. Yang and colleagues were also used PoPD as dopant for TiO_2 photocatalyst for the degradation of MB by using irradiation from 1000 W of Xe lamp. They observed no difference in peak locations and morphologies between the PoPD/ TiO_2 nanocomposite and pure TiO_2 ,

showing that the presence of PoPD had no effect on the TiO₂ lattice structure. However, photocatalytic activity of the composite was improved as 85.9% of MB was degraded, compared to 25.2% when pure TiO₂ was used. [17].

2.6 Modification of Catalyst

In general, the highly surface area of catalyst accelerates the reaction further and the surface area is greater in powder form compared to its solid form. However, due to nano-sized of particles, the loss of catalyst cannot be avoided after the treatment of wastewater. Therefore, many researchers were impregnating the catalyst on the support materials like polymers. Zaahari et. al. successfully impregnated BFO on the CMC membrane to degrade 91% of 10 ppm MO under direct sunlight within 180 min [63]. Meanwhile, Eutilério et al. synthesized Fe/Ag nanoparticles immobilized on polyacrylonitrile nanofibers (PAN NFs) for the purpose of decolorizing MO in synthetic water samples [77]. In addition to that, Hasmath Farzana fabricated TiO₂-chitosan beads to study the reduction of the heavy metal of Cr(VI) under the irradiation of the mercury lamp [78]. In contrast, Ridzuan et. al, used linear natural rubber (LNR) to impregnate BFO nanoparticles. They investigated the photocatalytic degradation of MB using the produced BFO-LNR thin film. It was found that, the removal of MB maintained above 94% even after the 5th cycle of reusability [79].

Generally, hydrogels are crosslinked networks of hydrophilic polymers which have a propensity to absorb a lot of water and swell without being soluble under physiological conditions of temperature, pH, and ionic strength [80]. Natural polymer-based hydrogels are preferred owing to their intrinsic biocompatibility and biodegradability, Additionally, natural polymers are less costly than synthetic polymers, thus, they are frequently used in the preparation of hydrogels. These natural

polymers include cellulose, starch, chitosan, sodium alginate, guar gum, gellan gum, and xanthan gum [81].

Polymers can be crosslinked both physically and chemically. When compared to chemically crosslinked hydrogels, the stability of physical crosslinked hydrogels is rather poor. In general, a crosslinking agent is required for chemical crosslinking processes via esterification reaction between the hydroxyl group (OH) and the carboxylic group (COOH) of acid [82] which results in crosslinking. Carboxymethyl cellulose (CMC), for example, is crosslinked by citric acid [71,81,83] maleic acid [50], and succinic acid [50], whereas chitosan is crosslinked by epichlorohydrin [84], genipin [85], and 1,4-dichlorobutane [86].

2.6.1 Carboxymethyl Cellulose (CMC) as Support Material

CMC is a cellulose derivative with a large number of carboxymethyl groups on the cellulose backbone. The presence of COOH and OH groups on cellulose renders it extremely soluble in water and chemically reactive; hence, CMC is frequently utilised as a hydrogel substrate. CMC has a good biocompatibility, biodegradability, and nontoxicity and high solubility in water [87], thus, it has a wide range of useful uses, including medical, food, papermaking, printing, and dyeing [82]. In order to minimise the problem of CMC dissolve in water during wastewater treatment, the hydrophilic CMC must be crosslinked to create a hydrogel using the crosslinking agent. The crosslinking mechanism of CMC is shown in Figure 2.3. According to Demitri et al. there are two main stages of the reaction of polyfunctional carboxylic acids with cellulose. Firstly, it is due to the attachment of the polyfunctional carboxylic acids via esterification with a cellulosic hydroxyl group. Secondly, it is further reaction via esterification with another cellulosic hydroxyl group producing a crosslink between cellulose chains. This mechanism is based on an anhydride intermediate formation.

Further reaction with a cellulose hydroxyl of another chain can then lead to crosslinking and causes the CMC to form a hydrogel that is not soluble in water [88].

Many researchers have explored composite hydrogels based on CMC, either in the form of thin film or beads; for example, Heidarpour and colleagues employed an Ag/AgCl photocatalyst within cross-linked CMC beads to treat RhB under visible sunlight [52], while Molly Thomas et. al. prepared crosslinked alginate/CMC with TiO₂-graphene oxide incorporation to treat CR under direct sunlight [89] and Ahmed Salama studied the removal of MB from waste water by using CMC-g-P (SPMA) super adsorbent hydrogels [90].

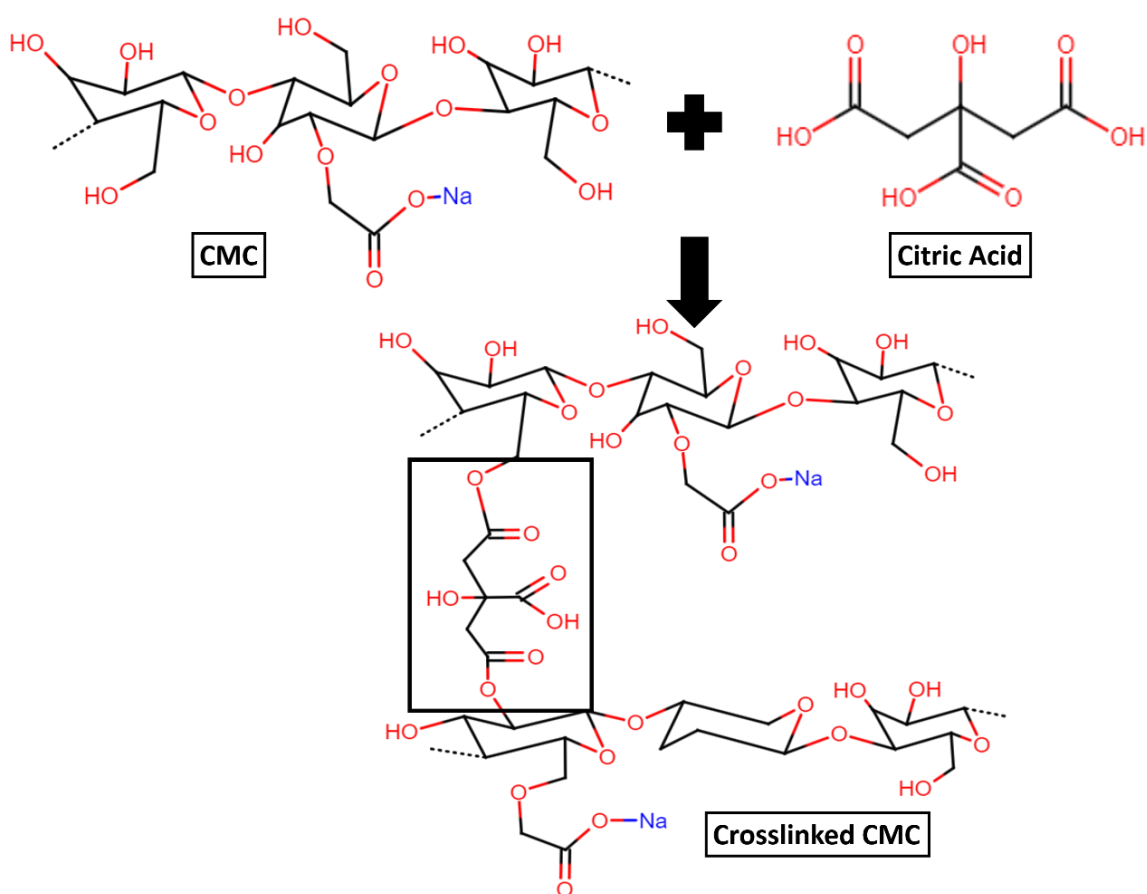


Figure 2.3 Mechanism of Crosslinked CMC

CHAPTER 3

METHODOLOGY

3.1 Experimental Flowchart

The research was divided into three parts. First, the preparation of CBP hydrogel film which began with the synthesis of BFO via biotemplate method, synthesis of BFO/PoPD composite by oxidative polymerization, followed by the impregnation of BFO/PoPD on the CMC hydrogel after the optimization of CMC hydrogel film was done.

The second part of the research was characterization of materials which are x-ray diffraction (XRD), x-ray photoelectron spectroscopy (XPS), Scanning Electron Microscopy with energy dispersive x-ray (SEM-EDX), thermogravimetric analysis (TGA), attenuated total reflectance-fourier transform infrared spectroscopy (ATR-FTIR), UV-vis diffuse reflectance spectroscopy (UV-vis DRS), determination of pH point of zero charge (pH_{PZC}) and material surface area and porosity.

The last part of the research was the application of the catalyst; photocatalytic degradation of MO. The optimization of BFO/PoPD was done by varying 3 parameters which are ratio of BFO:PoPD, concentration of HCl as the polymerization medium and ratio of APS:PoPD. After synthesis BFO/PoPD according to desire parameter, 0.01 g of the composite was loaded onto CMC hydrogel and the best condition was determined by testing its photocatalytic efficiency towards MO. In this part, 3 influence parameters were also studied; catalyst dosage, effect of initial concentration of Mo and effect of pH. Lastly, the reusability of catalyst was studied for 5 cycles. The experimental flowchart was summarized as in Figure 3.1.

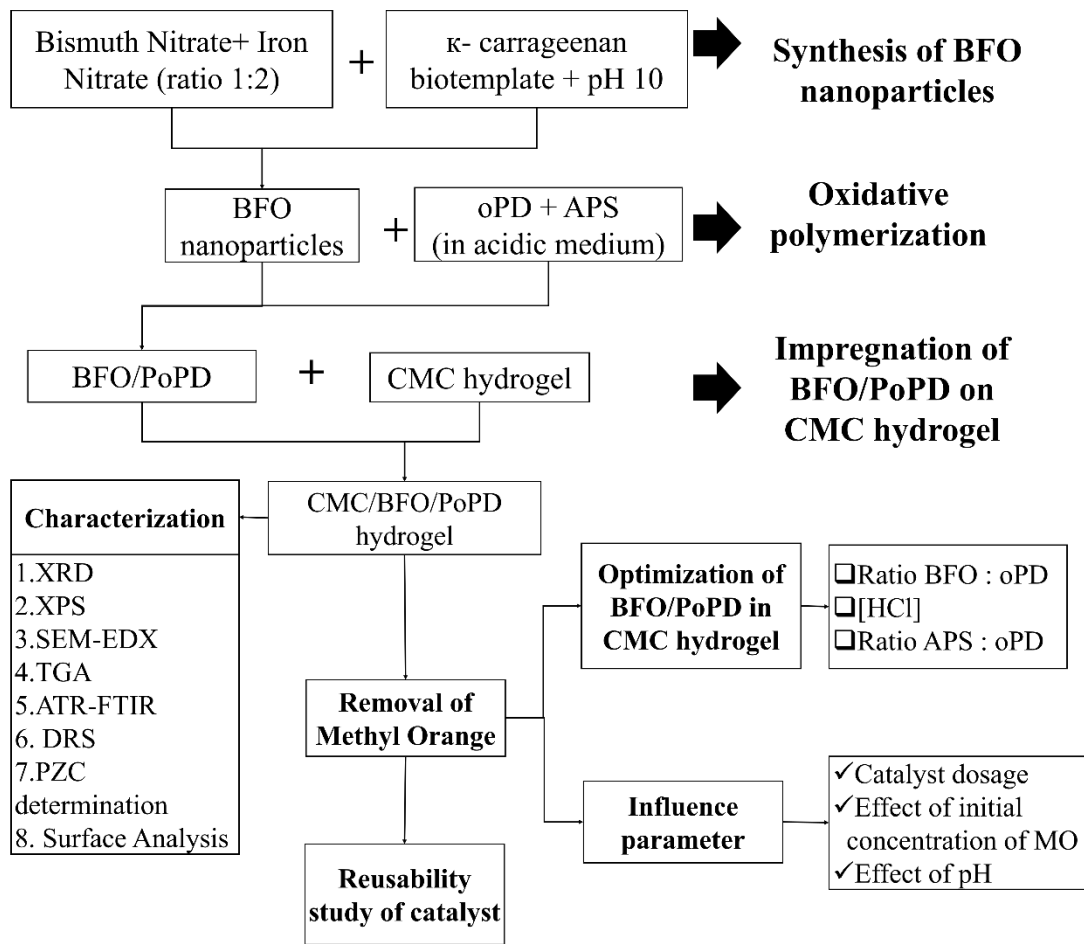


Figure 3.1 Experimental Flowchart

3.2 Chemicals and Reagents

Bismuth nitrate pentahydrate (98% purity) (Sigma-Aldrich), iron(III) nitrate nonahydrate (98% purity) (Sigma-Aldrich), κ -carrageenan (Sigma), ammonium persulphate (Sigma-Aldrich), o-phenylenediamine (Sigma-Aldrich), citric acid-1-hydrate (HmbG), carboxymethyl cellulose (Sigma), methyl orange dye (QReC), hydrochloric acid (HCl), and sodium hydroxide (NaOH). All the solutions were prepared by using distilled water.

3.3 Preparation of CMC/BFO/PoPD Hydrogel Film

3.3.1 Synthesis of BFO Catalyst by Biotemplating Method

BFO synthesis was carried out using the biotemplating process reported by previous study in our group [55,56]. Bismuth nitrate (1.42 g, 3.0 mmol), and iron nitrate (2.02 g, 0.5 mmol), were weighed and dissolved in 25 mL of distilled water to form 0.2 M precursor solution. This was followed by dissolving 5 mL of the precursor solution in 1% w/v of carrageenan solution. NaOH was used to alter the pH of the mixture to pH 10. For two hours, the light-yellow mixture was heated to 80 °C with vigorous stirring to ensure that all solvents were evaporated. The mixture was dried in an oven for overnight. The dry brown powders produced were calcined for two hours at 550 °C.

3.3.2 Synthesis of BFO/PoPD Composite by Oxidative Polymerization

0.012 M of o-phenylenediamine (oPD) was dissolved in 25 mL of 0.1 M HCl under constant stirring at room temperature. Then, 0.03 M (0.23g) of BFO was added into the solution. The mixture was sonicated for 15 mins to obtain a homogenized mixture. After that, 0.018 M of ammonium persulfate (APS) was dissolved in 7.97 mL of 0.1 M HCl and before added to the mixture of oPD/BFO in one portion and the mixture was quickly turned dark brown. The mixture was left at room temperature with agitation for 24 hours to allow oxidative polymerization to occur. Filtration and multiple washes with ethanol and distilled water were performed on the product until a colourless filtrate was produced. The precipitate was dried in the oven at 70° C for 12 hours and then, dark brown powder was obtained.

3.3.3 Optimization of BFO/PoPD Composite

The optimization of BFO/PoPD composite photocatalyst was conducted by varying the molar ratio of BFO to monomer oPD (1:1, 1:0.7, 1:0.4, and 1:0.1), concentration of HCl as polymerization medium (0.5 M, 0.3 M, 0.1 M, and 0.01 M) and molar ratio of initiator APS to oPD (1:2, 1:1, 1.5:1, and 1:2). 0.012 M oPD was dissolved in 50 ml 0.1 M HCl. The synthesized BFO/PoPD composites was impregnated on CMC film and the optimal composite condition for each parameter was found by carrying out photocatalytic degradation of MO, as discussed further in section 4.4.2.

3.3.4 Preparation of CMC Hydrogel Film

CMC film was prepared using 5% of commercial CMC and 2.5% of citric acid (CA) based on 25 mL of distilled water. CMC was added to the solution containing CA gradually under constant stirring for two hours to ensure the mixture was homogenized. Then, the mixture was poured into petri dish and dried in the oven at 40 °C for 48 hours. Then, the film was cured at 120 °C within 12 min. The round and clear film was obtained.

The optimization of CMC film was studied by the varying four parameters to enhance the hydrogel content; ratio of CMC to CA as the crosslinker, drying temperature, curing time and curing temperature. The hydrogel content of CMC was estimated by measuring its insoluble part in dried sample after immersion in distilled water for 24 h at room temperature. The obtained film was weighted (W_i), then it was soaked in distilled water for 24 h. The sample was then dried in the oven and weighted again (W_f). The gel fraction was then calculated as follows;

$$\text{Gel fraction \%} = (W_f/W_i) \times 100\% \quad (\text{Equation 3.1})$$